Journal of The Electrochemical Society, **155** (4) C138-C146 (2008)
0013-4651/2008/155(4)/C138/9/$23.00 © The Electrochemical Society

Multianalytical and In Situ Studies of Localized Corrosion of EN AW-3003 Alloy—Influence of Intermetallic Particles

A. Davoodi,[a,*] J. Pan,[a,,z] C. Leygraf,[a,**] and S. Norgren[b]**

[a]*Division of Corrosion Science, School of Chemical Science and Engineering, Royal Institute of Technology, SE-100 44 Stockholm, Sweden*
[b]*Sapa Technology, SE-612 81 Finspång, Sweden*

The influence of intermetallic particles (IMPs) on the localized corrosion behavior of an EN AW-3003 alloy was investigated in situ by conventional electrochemical measurements and high-resolution local probing techniques in chloride solutions with and without acetic acid. The open-circuit potential (OCP) fluctuations indicate local activities on the surface, and electrochemical impedance spectroscopy measurements suggest active dissolution in acidic solutions but a passivelike behavior in near-neutral solutions. Integrated atomic force microscopy/scanning electrochemical microscopy (AFM/SECM) was used to investigate the localized activities on the surface in a diluted chloride solution. The concurrent AFM and SECM images reveal cathodic activity of the IMPs and enhanced anodic current due to localized dissolution adjacent to some large IMPs upon anodic polarization. Moreover, in situ AFM imaging at OCP in solutions containing acetic acid show localized dissolution around the IMPs, leading to formation of deposits of ringlike corrosion products. The in situ observations reveal the microgalvanic effect of the IMPs, and the large IMPs are more prone to initiate localized corrosion compared to submicrometer dispersoids. Infrared absorption spectroscopy measurements after the exposure and thermodynamic calculations suggest the formation of mixtures of aluminum oxihydroxide and acetate on the surface in the presence of acetic acid.
 [DOI: 10.1149/1.2834454]

Manuscript submitted September 21, 2007; revised manuscript received November 15, 2007.
Available electronically January 31, 2008.

Aluminum alloys are interesting from different application perspectives such as for weight reduction in vehicles, household items, and constructions requiring high strength. A rolled EN AW-3003 alloy (European norm, aluminum wrought alloy), having Mn as the primary alloying element, is commonly used as the fin and tube material in heat exchanger applications in the automotive industry. The corrosion resistance is of increasing importance when the thickness of the material is scaled down to a level below 100 μm because of exposure to a corrosive environment such as deicing road salts. The influence of intermetallic particles (IMPs) on the resistance against localized corrosion is crucial for the material integrity in long-term service. The literature on corrosion studies of aluminum alloys has been reviewed in two papers[1,2] that point out the need to further explore the formation of pits at cathodic IMPs and the influence of second-phase particles. A recent survey of experimental data of electrochemical characteristics of IMPs in aluminum alloys collected by a microcapillary electrochemical cell shows that the corrosion potentials and pitting potentials vary over a wide range for various IMPs, and their electrochemical behavior is more complicated than the simple noble or active classification based on the corrosion potential or estimated from chemical composition.[3] IMPs capable of sustaining the largest cathodic current densities are not necessarily those with the noblest E_{corr}. Similarly, those with the least noble E_{corr} will not necessarily sustain the largest anodic currents.[3] Hence, not only thermodynamic but also kinetic aspects are important to consider when exploring the role of IMPs.

Various spectroscopic and microscopic techniques have been used to study the localized corrosion mechanisms of aluminum alloys. Electrochemical impedance spectroscopy (EIS) and electrochemical noise (EN) analysis have been used to investigate faradaic and capacitive characteristics of the interfacial regime of the aluminum surface and electrolyte.[4-8] Fourier transform infrared reflection absorption spectroscopy (IRAS) has been used to determine the corrosion products formed on aluminum alloys, both in atmospheric and aqueous corrosion.[9-14] These spectroscopic techniques provide data that are helpful to understand the complex processes, but the information, due to lack of lateral resolution, cannot be directly related to the microstructural features of the alloys. With state-of-the-art microscopic techniques, microstructural features such as IMPs in aluminum alloys can be characterized in more detail. Mapping of the Volta potential of the alloy surface using scanning Kelvin probe force microscopy (SKPFM) is of particular interest from a corrosion point of view.[15-18] Because the Volta potential is related to the corrosion potential and is regarded as a measure of practical nobility, and SKPFM provides local potential data with high spatial resolution, such information is helpful for detailed mechanistic studies of local corrosion. The limitations of SKPFM for surface analysis of aluminum alloys were discussed recently,[15,16] emphasizing the precautions needed in quantitative interpretation of the potential data.

One approach with great promise is to use high-resolution microscopy for in situ observation of morphology changes during ongoing corrosion processes,[19-23] in particular if the microscope can be altered to allow local electrochemical studies as well.[24-26] Scanning electrochemical microscopy (SECM) has been used to spatially resolve the heterogeneous cathodic activity at AA2024 surfaces in an organic solution. The images show locally distributed high redox reactivity correlated with the locations of the IMPs.[22] Trenching and cavity formation have been observed around various types of IMPs on AA2024-T3 both at an open-circuit potential (OCP) and at more negative potentials in the absence of Cl^-, demonstrating that both the Cu-rich and Fe-rich IMPs can serve as cathodes for O_2 reduction.[27] Complementary with fluorescence and near-field scanning optical microscopy, SECM showed that the cathodic reaction on AA2024 was limited to the surface area of IMPs.[23] Recently, we have used integrated atomic force microscopy (AFM)/SECM for in situ studies of localized corrosion of aluminum alloys to obtain concurrent topography and electrochemical activity variations on the very same surface area, showing ongoing localized corrosion activities.[24-26]

In this work, OCP and EIS measurements were performed to investigate the overall corrosion behavior of rolled EN AW-3003 in neutral and acidic chloride solutions. Furthermore, an integrated AFM/SECM was used to detect localized corrosion activity related to IMPs, and in situ AFM imaging was used to monitor the local corrosion attack and formation of corrosion products. Moreover, IRAS analysis of the sample surface after exposure was carried out to identify the chemical components of the corrosion products. Thermodynamic calculations of the dominant chemical species for the system were also performed, providing support for the presence of

* Electrochemical Society Student Member.
** Electrochemical Society Active Member.
z E-mail: jinshanp@kth.se

corrosion products detected by IRAS. More detailed results of Volta potential data and in situ observations of the localized corrosion processes are reported in a parallel paper.[28]

Experimental

Sample material and preparation.— The chemical composition (in weight percent) of the EN-AW3003 alloy is as follows: 1.1% Mn, 0.48% Fe, 0.15% Si, 0.12% Cu, 0.03% Mg, $<0.01\%$ Zn, and Al as the balance. Prior to hot rolling, the alloy was submitted to a homogenization heat-treatment. After this, normal practices for cold rolling were employed, including an annealing step and a final reduction. For traditional electrochemical measurements, the as-received surface was cleaned by ethanol before the experiments. For microstructural characterization and local electrochemical measurements, small samples (section of 1.0×0.1 mm) were cut and embedded in epoxy. The surface investigated was sectioned longitudinally to the rolling direction. The sample was ground and polished following normal procedures for scanning electron microscopy (SEM) analysis, with a final polishing step using a colloidal silica suspension at about pH 10, and was subsequently cleaned in ethanol and dried in air. Acetone was avoided during sample preparation because it was reported that severe pitting might be induced by acetone together with a layer of chloride solution.[29,30]

SEM-EDS analysis of IMPs.— A standard SEM/EDS instrument, a Philips XL305 field emission gun scanning electron microscope, was used for microstructural characterization and composition analysis of the IMPs. Backscattering SEM images were obtained to visualize the contrast between IMPs (higher density) and the alloy matrix. Selected large-constituent IMPs were analyzed individually by energy-dispersive X-ray spectroscopy (EDS), taking into account the contribution from the alloy matrix, whereas nanosized dispersoids were analyzed spot by spot or after etching away the matrix. The composition so obtained should be regarded as an approximation of the IMPs.

Corrosion test solutions.— Corrosion testing of the samples was performed in chloride-containing solutions ranging from mild to aggressive: (*i*) a diluted 10 mM (0.06 wt %) NaCl, (*ii*) 3.5 wt % NaCl, and (*iii*) a corrosive solution (4.2 wt % artificial sea salt + 0.6 wt % CH_3COOH) used in accelerated tests according to ASTM G-85 with the ASTM D1141 solution (Annex A3 without heavy metals), i.e., artificial ocean water acidified with acetic acid to pH 2.9, established as the seawater acidic accelerated test (SWAAT), and hereby the solution is denoted as the SWAAT solution. The last solution is interesting from an application point of view, because it can give a rapid and qualitative evolution of the influence of alloying elements on aluminum alloys in heat-exchanger applications, and related galvanic compatibility issues. For the in situ AFM measurements, however, this solution was used as supplied and also adjusted to about pH 4.0 to avoid a too fast dissolution. The intention of the corrosion test solutions was to imitate different environments and real corrosion situations. Reagent chemicals of analytical grade and distilled water were used to comprise the solutions, except for the SWAAT solution, which was supplied by Sapa Technology.

OCP and EIS measurements.— To investigate the overall corrosion behavior and characterize the alloy–solution interface, OCP and EIS measurements were performed for the alloy in the solutions at different exposure times. The measurements were repeated at least three times. A standard three-electrode cell with a Pt counter electrode and a saturated Ag/AgCl reference electrode was used for the electrochemical measurements, together with a potentiostat Solartron 1287 and a frequency response analyzer Solartron 1255. EIS was performed at the OCP with an ac amplitude of 10 mV. ZView (Scribner Associates, Inc.) software was used for analysis of the EIS spectra.

Integrated AFM/SECM and in situ AFM measurements.— For visualizing local corrosion activity occurring on the alloy surface, i.e., anodic or cathodic reaction sites, the integrated AFM/SECM measurements were performed at OCP and at cathodic or anodic polarization. For this purpose, a diluted solution (ca. pH 6.0) of 10 mM NaCl was used to avoid extensive corrosion so that individual local events could be resolved. In addition, either 5 mM KI or 2 mM $K_4Fe(CN)_6$ was added as a redox mediator for the SECM mapping of electrochemical current in the solution. A small electrochemical cell made of Teflon was used, with a solution layer of ca. 1.5 mm in thickness covering the sample surface. A saturated Ag/AgCl was used as the reference electrode and a Pt foil surrounding the sample was used as the counter electrode. Moreover, to monitor the surface change due to localized corrosion on the alloy surface, in situ AFM measurements were performed after prolonged times of exposure in the solutions, including the aggressive one (SWAAT solutions at pH 2.9 and 4.0) at different time intervals.

For the integrated AFM/SECM and in situ AFM measurements, the instrument used was a Resolver from Quesant, Ltd., equipped with the iProbe package supplied by Windsor Scientific, Ltd., U.K. The in situ AFM was performed using a standard SiN cantilever. Details of the AFM/SECM instrument have been described previously.[24-26] In short, the integrated AFM/SCEM was performed using a dual-mode cantilever/tip probe, and the SECM was operated in the sample-generator-tip-collector mode using the redox mediator. During the measurement, the sample was held at OCP or polarized, while the microelectrode in the dual-mode probe was controlled at a predefined potential to collect local current through the redox reaction of the mediator. By scanning over the surface, concurrent AFM topography and SECM current maps were obtained of the same area. The lateral resolution of the SECM depends on the tip size and geometry, the sample-tip distance, and the electrolyte conductivity. Simulation, characterization, and verification of the AFM-based SECM are reported elsewhere.[31]

IRAS analysis of corrosion products.— In an effort to identify the corrosion products formed on the surface (observed by in situ AFM), IRAS spectra were obtained ex situ for the sample after exposure in the aggressive SWAAT solution. The sample was taken out from the solution and dried gently by N_2 gas blowing along the sample surface before placing it into the IRAS chamber. The analysis was performed by using a Digilab FTS 40 Pro spectrometer with a mercury cadmium detector by applying a p-polarized light and averaging 1024 scans at a resolution of 8 cm^{-1} in the range 500 – 4000 cm^{-1} on a 1 cm^2 sample area. The spectra were recorded in absorbance units ($-\log R/R_0$), where R is the reflectance of the exposed sample and R_0 is the background reflectance obtained from a polished surface after 1 h in dry air (RH $< 0.1\%$).

Thermodynamic calculation of chemical compounds in corrosion products.— As complementary information regarding the corrosion products that may form on the alloy surface during the corrosion tests, thermodynamic calculations of predominant species (Pourbaix diagram) and species distribution (fraction) were performed for possible chemical compounds of aluminum in the test solution by using the Hydra/Medusa Chemical equilibrium software.[32] The solubility and thermodynamic stability of the species at 25°C were considered in the calculation to identify the species distribution for chemical compounds of aluminum. A potential at −0.6 V vs a normal hydrogen reference electrode (NHE) was chosen for the calculation of the species distribution, which is approximately the level of OCP of the alloy in the test solutions.

Results and Discussion

SEM/EDS analysis of IMPs.— The SEM/EDS analysis was made on the sections longitudinal to the rolling direction of the samples. Figure 1 shows a typical backscattering SEM image of sections in the longitudinal direction. IMPs appear brighter in the images due to their higher density compared to the Al matrix. EDS analysis of larger constituent particles (>2 μm) showed that the EN AW-3003 alloy mainly contains particles of $Al_6(Mn,Fe)$ type

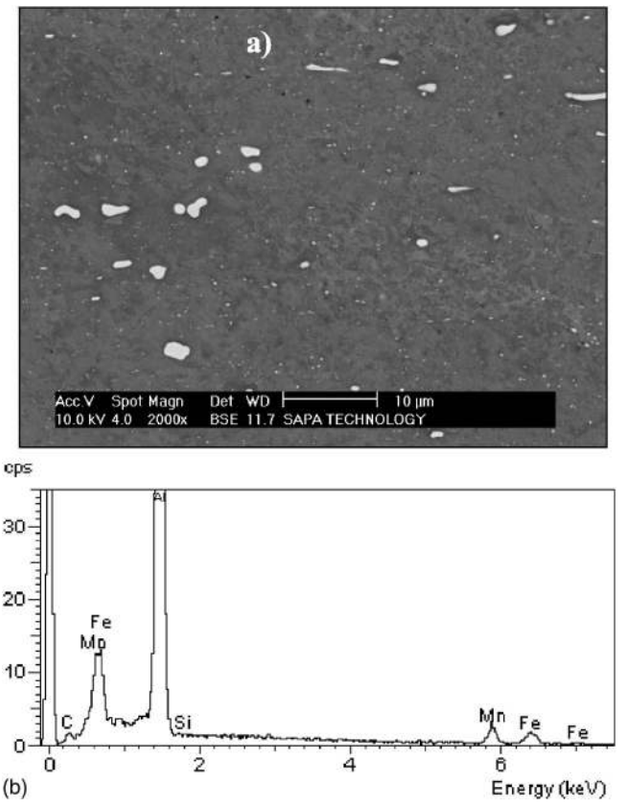

Figure 1. (a) Backscattering SEM image of a polished cross section of the EN AW-3003, and IMPs (large constituents and small dispersoids) appear bright in the image. (b) EDS analysis of a large constituent IMP containing Mn and Fe.

and some of $Al_{12}(Mn, Fe)_3Si$ type, in both cases with a Mn/Fe ratio of about 1:1. There is also a high density of fine particles appearing as white dots, known as dispersoids. The fine dispersoids of 0.5 μm size or less normally have the composition $Al_{12}Mn_3Si_{1-2}$. More detailed results were described in the parallel paper.[28]

OCP vs time of exposure.— The OCP measurements were performed on a 1 cm^2 surface area exposed to the solutions, with 1 data point/s. Figure 2 shows typical examples of the results for the alloy during the first hour of exposure to the solutions. The OCP

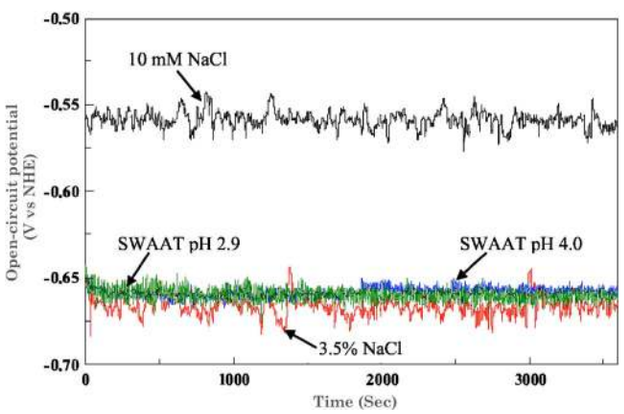

Figure 2. (Color online) OCP vs time for EN AW-3003 alloy during the first hour of exposure to 10 mM NaCl, 3.5 wt % NaCl, and SWAAT at pH 4.0 and pH 2.9, respectively.

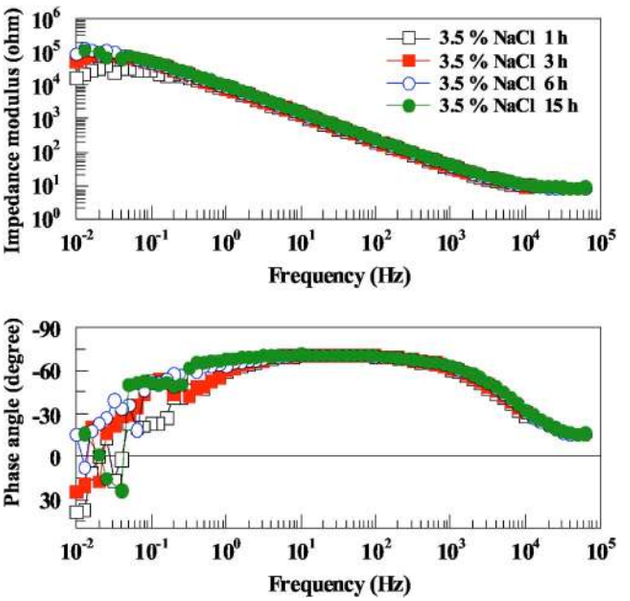

Figure 3. (Color online) Bode plots for EN AW-3003 exposed to 3.5 wt % NaCl for 1, 3, 6, and 15 h, respectively.

remains nearly the same during the whole exposure time, whereas the level is lower for higher NaCl content, probably due to many active sites on the alloy surface. More importantly, the results show potential fluctuations during the exposure, especially in the near-neutral chloride solutions. With a prolonged exposure, some large potential drops were observed for the 3.5 wt % NaCl solution. The number of the fluctuations and extent of the potential fluctuation appear to be influenced by the chloride content and pH of the solution. The OCP level is almost the same in SWAAT solutions at pH 2.9 and 4.0, and the magnitude of fluctuations is smaller but the frequency (number) of fluctuations apparently is higher as compared to the near-neutral chloride solutions. The influence of pH may be explained by the dominant cathodic reaction. At low pH, proton reduction is the dominating cathodic reaction occurring on an activelike alloy surface, whereas in near-neutral solutions oxygen reduction is the dominating cathodic reaction occurring on a passivelike alloy surface. These observations indicate local activation processes occurring in the vicinity of IMPs, which are revealed by the integrated AFM/SECM measurements (see below). Other authors also observed potential and current fluctuations by EN measurements of pure aluminum in 0.05 M NaCl close to its pitting potential which were attributed to electrochemical processes within active pits and electrochemical interactions between the active pits.[8]

EIS characterization of alloy–solution interfaces.— EIS measurements were performed on a 1 cm^2 surface area after different times of exposure in the solutions to characterize interfacial properties of the alloy–solution interfaces. Figure 3 shows typical Bode plots of the spectra obtained in a 3.5 wt % NaCl solution. From high frequency down to around 0.1 Hz, the spectra exhibit one time constant feature (one semicircle in Nyquist plot). As can be seen, the impedance in this frequency range increased slightly with exposure time and stabilized after a few hours of exposure, which is an indication of a certain passivation process of the alloy. This suggests that the surface tends to form some protective surface film (e.g., an aluminum oxihydroxide) in this near-neutral solution. However, at low frequencies (<0.1 Hz), the data become scattered and indicate an inductive response. The scattering could not be avoided by adjusting the measuring setup and is not due to too high impedance of the system. Most likely this scattering is caused by electrochemical fluctuations of the interface, as evidenced by the OCP vs time

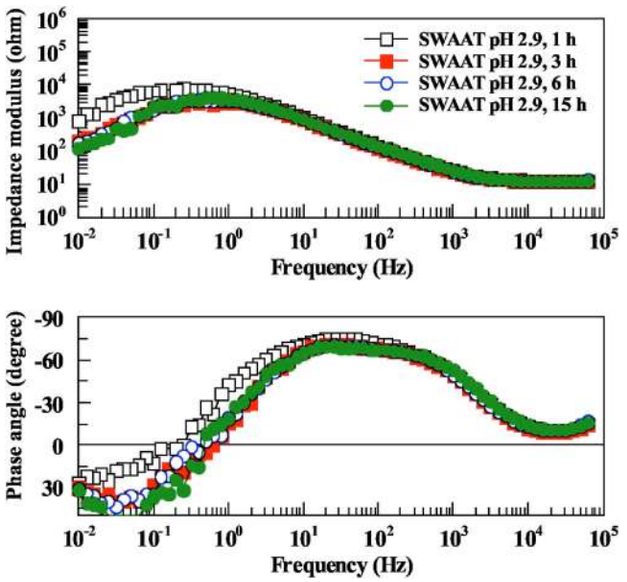

Figure 4. (Color online) Bode plots for EN AW-3003 exposed to SWAAT solution at pH 2.9 for 1, 3, 6, and 15 h, respectively.

curves. The EIS spectra obtained in a 10 mM NaCl solution show similar features as in the 3.5 wt % NaCl solution. The main difference is that the impedance in the medium-frequency range is somewhat higher for the 10 mM NaCl solution than it is for the 3.5% NaCl solution.

The EIS spectra for the alloy exposed to the aggressive SWAAT solutions reveal a different behavior compared to the near-neutral chloride solutions. As an example, Fig. 4 shows typical Bode plots obtained in the SWAAT solution at pH 2.9. The impedance in the high- and medium-frequency range is lower and decreases slightly with exposure time during the initial period (several hours), which is in contrast to the trend in the near-neutral solutions. The scattering of low-frequency data starts to occur at around 1 Hz, and the inductive response at low frequencies is more pronounced than in the near-neutral chloride solutions, which can be better viewed in Nyquist plots. The spectra obtained in the SWAAT solution at pH 4.0 are similar to those obtained in the SWAAT solution at pH 2.9, except that the impedance at low frequencies is not as low as in the case of pH 2.9. The results indicate many active sites (a more active surface) in this more aggressive solution, which is in accordance with a large number of potential fluctuations with small magnitudes observed in the OCP measurements. The local active sites are most likely due to the presence of IMPs, which are revealed by the in situ AFM measurements (see later section).

The interpretation of impedance diagrams of pure aluminum in acid and neutral environments is difficult when it is based only on EIS measurements. In literature, it has been proposed that the high-frequency response is probably related to the formation of the oxide layer, and the low-frequency response may be assigned to the dissolution of the oxide, while the inductive behavior may be related to adsorbed species.[6] For a detailed analysis, one has to take into account all possible reactions.[7] The behavior of pure aluminum in 0.1 M KCl without and with the acetate buffer at pH 5.4 and 4.3 has been studied by EN and EIS, and it was also observed that the impedance decreases with time during several hours.[4] The instability and variation of the local potential was explained by the presence of metastable pits on the surface. The EN analyses in the frequency domain are in good agreement with those obtained by EIS, suggesting that the presence of acetate increases the corrosion rate of aluminum. Unfortunately the low-frequency data were missing in the report.

The EIS results obtained in this work provide similar information as reported in literature. The high- and medium-frequency data suggest oxide formation in the near-neutral solutions but active dissolution in the aggressive solution at lower pH. The low-frequency data, including the inductive response, suggest a certain degree of localized dissolution occurring on the surface in both the near-neutral solutions and the aggressive solution at lower pH, with a greater extent for the latter. In this work, no effort was made to perform complicated spectra fitting to obtained quantitative data from the EIS spectra. Instead, by taking advantage of state-of-the-art local-probing techniques, the main work was focused on in situ experiments to obtain direct evidence of localized corrosion processes related to IMPs.

Integrated AFM/SECM observation of local electrochemical activity.— Although SKPFM (ex situ technique) can provide useful information that indicates the cathodic character of large IMPs relative to the alloy matrix,[26,28] corrosion is a process that also depends on the surrounding environment, so that in situ techniques are needed to obtain direct evidence for the influence of IMPs on the localized corrosion. Hence, the approach in this study is to investigate in situ localized corrosion processes using an integrated AFM/SECM[24-26] capable of visualizing local electrochemical activities on the surface with micrometer resolution while following the surface topography change during ongoing corrosion processes. This enables observation of local processes, such as prepitting events, before and while topographic changes occur. Here selected examples are given, and detailed results are reported elsewhere.[26,28]

For the SECM imaging, the sample can be controlled either at cathodic or anodic potentials to visualize local electrochemical activities on the surface. Figure 5 shows concurrent AFM and SECM images for the alloy exposed to a 10 mM NaCl + 2 mM $K_4Fe(CN)_6$ solution with 200 mV cathodic polarization. In this case, the local enhanced current is due to cathodic reactions of the mediator and/or reduction of dissolved O_2 in the solution. The images in Fig. 5 were obtained in the first successful effort and the quality may eventually be improved in future studies. The higher areas in the AFM topography image are likely the sites of the large IMPs, as judged from their size and the shape (after polishing IMPs appear higher because they are harder than the matrix), and a few sites with local enhanced cathodic current were observed in the SECM image of the same surface area. Interestingly, the high local current sites correlate well with the locations of higher areas (IMPs), but not all of the higher areas exhibit enhanced current. This implies that interference between the topography and the current signals is not an issue of concern in the measurements. The results provide direct evidence of enhanced cathodic activities on the surface that can be correlated with the IMPs, and also demonstrate that not all of the large IMPs exhibit enhanced cathodic activity. It was earlier reported by other authors that, by comparing SECM images of quite low lateral resolution with SEM micrographs of the same area, regions of high redox reactivity were related to the locations of IMPs.[22,27]

Figure 6 shows an SECM image of the alloy exposed to 10 mM NaCl + 5 mM KI (mediator) with 100 mV anodic polarization, where overall the sample is in the passive potential region in this solution. In this case, the local enhanced current is due to local anodic processes occurring on the alloy surface. Because it took several minutes to acquire such an image, the local high current shows some quite "stable" electrochemical processes rather than transit events that disappear quickly. Here the surface was still very smooth (like polished) and the concurrent AFM topography image did not reveal any noticeable change. Figure 7 shows concurrent AFM and SECM images for the alloy exposed to 10 mM NaCl + 5 mM KI with 200 mV anodic polarization under which passivity breakdown occurs. The SECM image shows local electrochemical activities due to the localized dissolution at this potential, and the AFM topography image reveals simultaneous topography changes on the surface (early pits). Note that here local high current does not necessarily appear on the location of the pits, because pits are

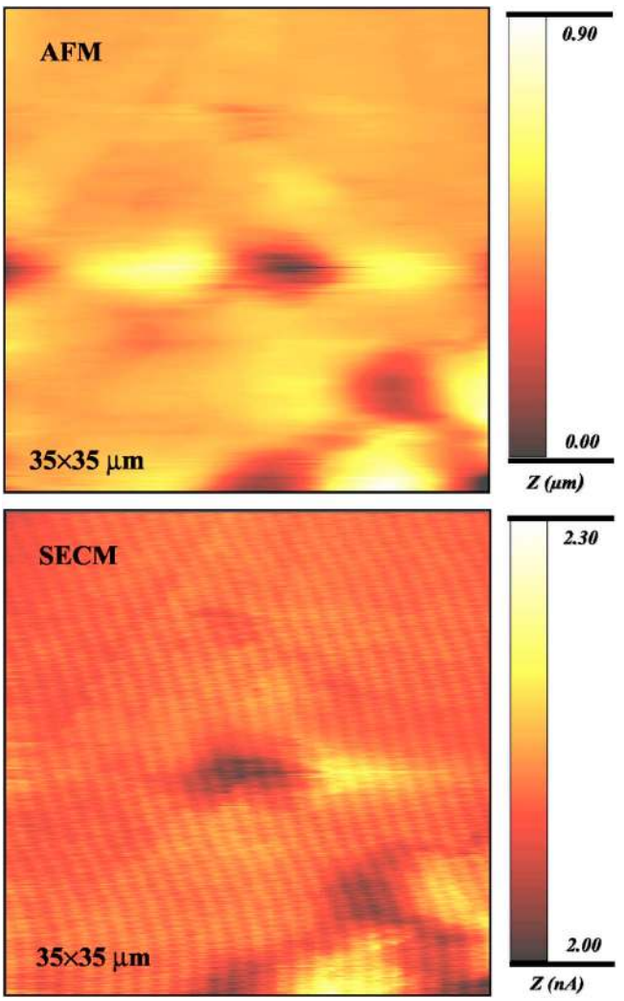

Figure 5. (Color online) Concurrent AFM and SECM images of EN AW-3003 alloy exposed to 10 mM NaCl + 2 mM $K_4Fe(CN)_6$ as a mediator, with 200 mV cathodic polarization.

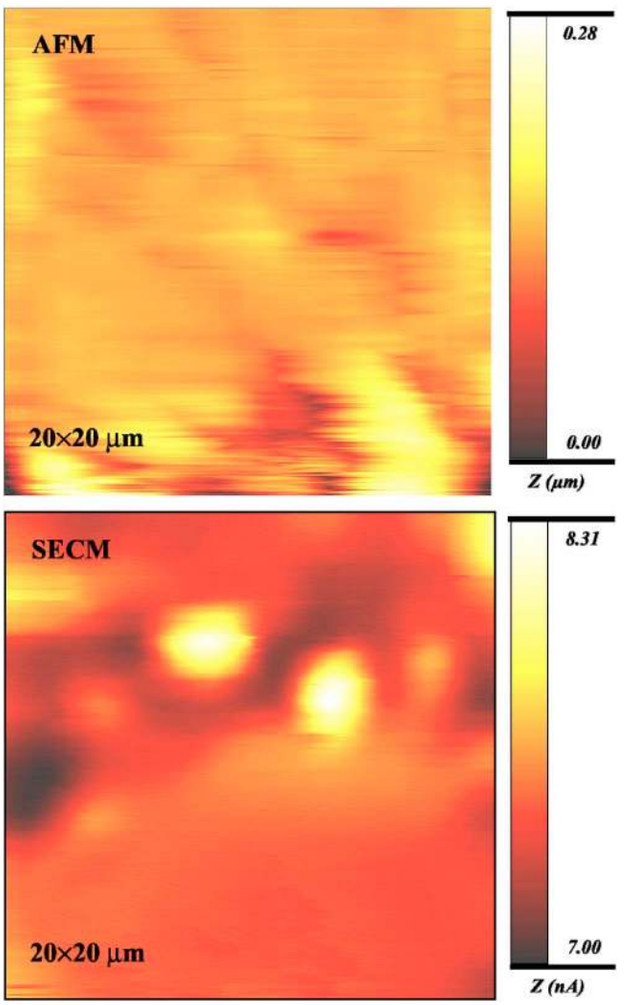

Figure 6. (Color online) Concurrent AFM and SECM images of EN AW-3003 alloy exposed to 10 mM NaCl + 5 mM KI (mediator), with 100 mV anodic polarization. The images were obtained within ca. 10 min of the anodic polarization.

formed after substantial local dissolution has occurred, and the anodic current may vanish when the pits stop developing. Although the quality of the AFM topography image obtained in the integrated mode is not as good as can be achieved by a standard AFM probe,[26] judging by the size and shape of the areas of higher current, the local active sites are likely related to IMPs. This is more clear in Fig. 8, which shows two sequential SECM images (ca. 35 min in between) with elongated areas of high-current area resembling some large IMPs. The sequential images were obtained by switching off the feedback control of the distance between the sample and tip to make fast data acquisition, i.e., performing measurements in normal SECM mode. It is interesting that both maximum (light) and minimum (dark) anodic activities can be seen, which can be related to the active sites and an inactive area at that vicinity, respectively. The SECM images in Fig. 8 also reveal the dynamic character of localized corrosion on the alloy surface.[26]

In short, the integrated AFM/SECM measurements at both cathodic and anodic polarizations reveal enhanced cathodic activity on the surface of some large IMPs and enhanced anodic dissolution in the vicinity of some large IMPs. The results provide direct evidence of cathodic action of the large IMPs in localized corrosion of the aluminum alloy.

In situ AFM observation of localized corrosion.— Detailed localized corrosion processes, both formation/growth of pits and deposition of corrosion products, were observed in situ by AFM imaging of the alloy surface in the solutions. The extent of localized corrosion was influenced by the solution, and the number of local dissolution events is smaller in the near-neutral chloride solutions than in the aggressive SWAAT solution, where extensive local dissolution and deposition of corrosion products occurred after several hours of exposure in pH 2.9, and after 2–3 days in pH 4.0. Figure 9 shows examples of the in situ AFM images obtained on different surface areas, displaying pit formation, local dissolution around large IMPs, and the crystallographic features of the local dissolution, after several hours of exposure in the SWAAT solution at pH 2.9. The large IMPs appear lighter in the AFM topography images. The results indicate that localized dissolution often occurs in the boundary region adjacent to large IMPs (Fig. 9b), and pits seem to grow preferentially in between large IMPs (Fig. 9c). Moreover, crystallographic dissolution was also observed (Fig. 9d), similar to that reported previously,[33] probably related to triple grain boundary points. The localized dissolution can be explained by galvanic effects between the IMPs and the alloy matrix, which enhance the anodic dissolution of the alloy matrix in the vicinity of the IMPs due to the cathodic action of the IMPs, as discussed in the previous section. The locations between nearby large IMPs are preferential sites for pit development, because the local kinetic conditions with

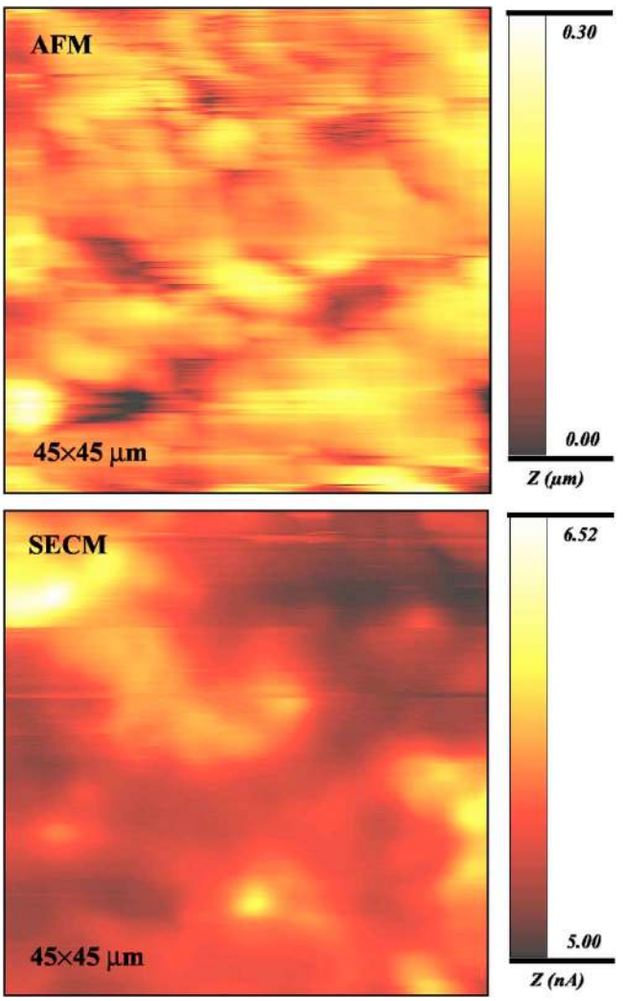

Figure 7. (Color online) Concurrent AFM and SECM images of EN W-3003 alloy exposed to 10 mM NaCl + 5 mM KI as a mediator, with 200 mV anodic polarization. The images were obtained within ca. 10 min of the anodic polarization.

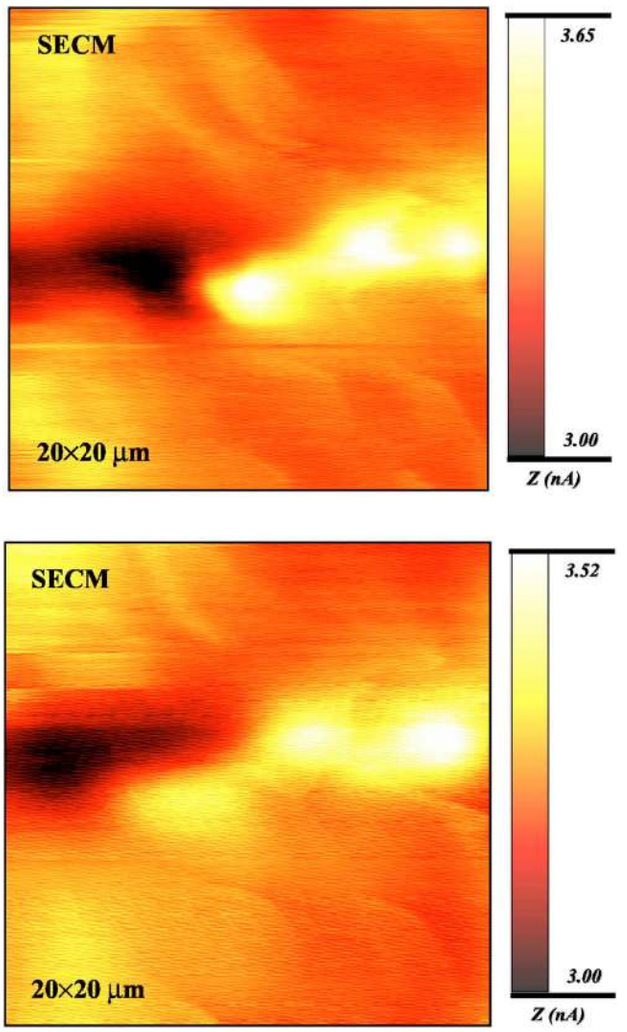

Figure 8. (Color online) Two sequential SECM images at the same area of EN W-3003 alloy exposed to 10 mM NaCl + 5 mM KI, with 200 mV anodic polarization. The time interval between the two images was ca. 35 min.

coupled cathodic reactions on the IMPs favor a sustainable local dissolution at these sites. The cathodic character of the large IMPs was previously revealed by ex situ Volta potential mapping, and the cathodic activity was demonstrated directly by integrated AFM/SECM measurements.[26,28] Not all large IMPs initiate localized dissolution and pitting (see, for example, the image in Fig. 9c). The observation suggests that not only thermodynamic but also kinetic conditions are crucial for the localized corrosion to proceed, emphasizing the need for in situ studies of the role of IMPs.

The in situ AFM images in Fig. 10 show extensive deposition of corrosion products on the alloy surface in the SWAAT solution at pH 4.0, which often surround large IMPs. More details of the corrosion products were reported previously,[26] showing deposits consisting of clusters of micrometer-sized crystals. As can be seen in Fig. 10b, the corrosion products assemble in a regular manner, creating a ringlike shape, and accumulate in several sequences. Such extensive local dissolution and deposition of corrosion products was observed in situ on the EN AW-3003 alloy after only a few days of exposure in the aggressive SWAAT solution at pH 4. The deposition of the corrosion products can be explained as follows: the enhanced local dissolution around large IMPs results in a local high concentration of Al ions, and the cathodic reaction (reduction of dissolved O_2) on top of large IMPs leads to a local high concentration of hydroxyl ions in the vicinity of the IMPs, despite the low pH of the bulk solution, as "local alkalization" proposed previously by other authors.[34,35] As a result, local saturation of dissolved Al ions and hydroxyl ions generates the deposits of corrosion products surrounding the large IMPs, mainly as Al hydroxides but also acetate complexes, as evidenced by subsequent surface analysis and thermodynamic calculations. The crystalline feature (brick shape[26]) of the smallest units of corrosion products observed by in situ AFM also indicates that they are formed through deposition from the saturated solution.

Fourier transform infrared-IRAS analysis of corrosion products.— In order to identify the corrosion products formed on the surface shown above, IRAS spectra were obtained ex situ of the alloy surface after exposure to the SWAAT solution at pH 4.0 for 4 and 28 h (Fig. 11). Although transfer of the sample from the aqueous solution to the IRAS chamber may cause some change in the chemical composition of the corrosion products, e.g., loss of water and hydroxides, the IRAS results can give information about the identities of the corrosion products that form and strongly adhere the surface. As can be seen in Fig. 11, the IRAS spectra show an increasing intensity of stretching vibrations with exposure time. The peak assignment is shown in Fig. 11 for the spectrum taken after 28 h of expo-

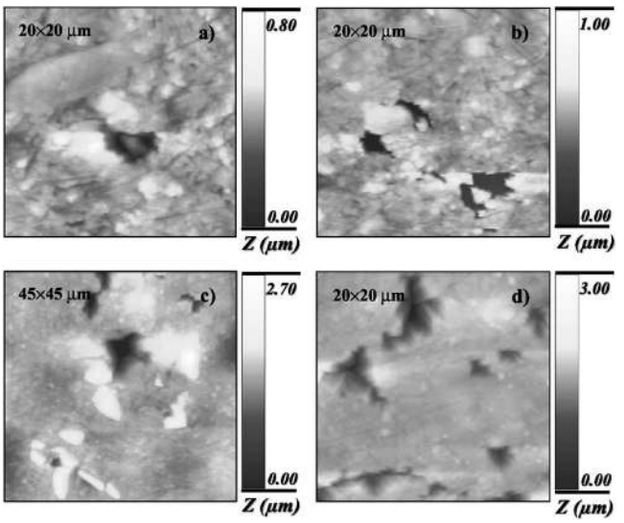

Figure 9. In situ AFM images of EN AW-3003 alloy in a SWAAT solution with pH 2.9 after a certain time of exposure: (a) an early pit (120 min), (b) local dissolution around IMPs (150 min), (c) deep pits between IMPs (170 min), and (d) crystallographic dissolution (190 min).

sure. The peaks can be assigned to a stretching vibration of the Al–O band (629 – 700 cm^{-1}), a stretching vibration of the Al–OH band (~1129 cm^{-1}), and symmetric and asymmetric vibrations of the $COOH^-$ band (~1472 and 1602 cm^{-1}).[10-14] Because the sample was dried before the analysis, only a broad weak peak was found at around 3500 cm^{-1}, which is associated with absorbed water or hydroxyl groups. It is not possible to ascertain any peak associated with aluminum chloride components (direct Al–Cl peaks at wavenumbers too low to be seen by IRAS). The results indicate that some mixture or complex of oxides, hydroxides, and acetate of aluminum are formed and accumulate gradually with exposure to the aggressive SWAAT solution. The analysis results provide evidence that oxides, hydroxides, and acetate of aluminum were formed on the alloy surface as a result of the enhanced local dissolution processes shown above and concomitant reactions of dissolved aluminum ions and anionic species of the SWAAT solution. However, it is difficult to determine more precisely the composition of the compounds in the corrosion products by means of IRAS.[36] This has motivated the thermodynamic calculations as presented below.

Thermodynamic calculations.— In order to find the thermodynamically based dominant region of aluminum compounds in the SWAAT solution, Pourbaix diagrams were drawn by using the Medusa software[32] for aqueous solution containing 0.01–1 M NaCl and 0.1–1 M acetic acid (CH_3COOH) to cover the range of test solutions. The calculation takes into account all major dissolved species and solid compounds that may exist in the system, including $AlOH^{2+}$, $Al(OH)_2^+$, $Al(OH)_3$, $Al(OH)_4^-$, $Al(OH)_3(c)$, AlOOH(c), $Al(CH_3OOH)^{2+}$, CH_3COOH, CH_3COO^-, $Al(OH)(CH_3OOH)^+$, $Al_2(OH)_2(CH_3OOH)^{3+}$, $[Al(H_2O)_6]^{3+}$, $[Al(H_2O)_4(CH_3COO)_2]^-$, $Na(CH_3COOH)$, NaCl, and $AlCl_3$, where c denotes a crystalline solid. The calculation is simplified with respect to the SWAAT solution containing artificial sea salt with undefined minor species. The database used may not include all possible species because of lack of thermodynamic data of some intermediate species.

The calculations show that the stability regions deduced are affected by the contents of NaCl and acetic acid. As an example, Fig. 12 displays the Pourbaix diagram (Fig. 12a) obtained with 1.0 M NaCl and 0.1 M CH_3COOH (similar to the SWAAT solution), which shows the stability region for aluminum in the aqueous system. The species distribution (fraction) obtained at −0.6 V vs NHE is shown in Fig. 12b for different dominant aluminum compounds existing in

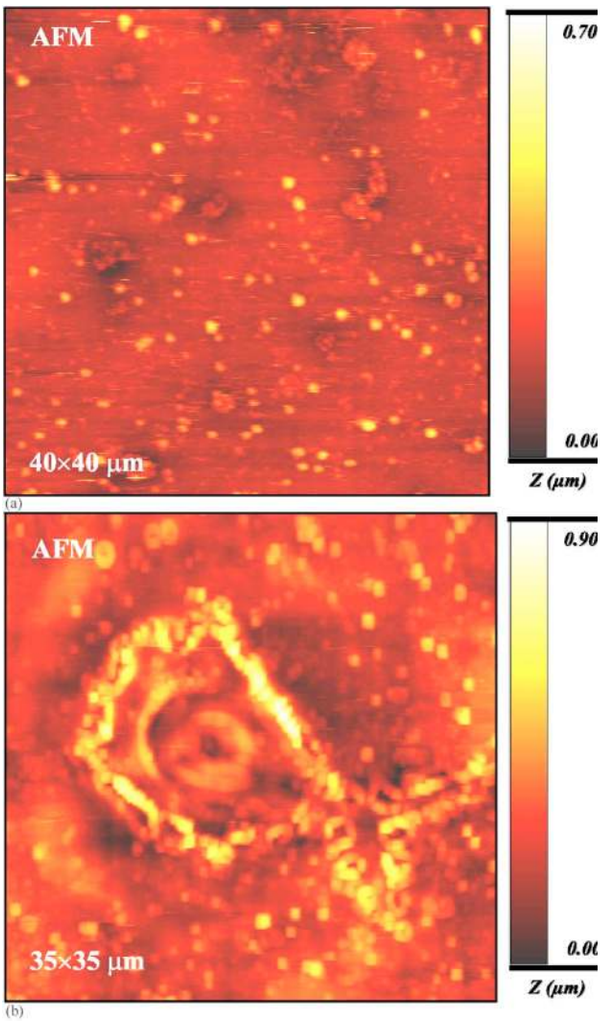

Figure 10. (Color online) (Color online) In situ AFM images of EN AW-3003 alloy in a SWAAT solution at pH 4.0 after (a) 2 and (b) 3 days, showing deposition of corrosion products.

the solution from pH 2 to 8. As can be seen in Fig. 12a, $AlCl_3$ is dominant when pH is below 3.5, $Al(CH_3COOH)^{2+}$ is dominant between pH 3.5 and 3.8, whereas $Al(OH)(CH_3COOH)^+$ is dominant

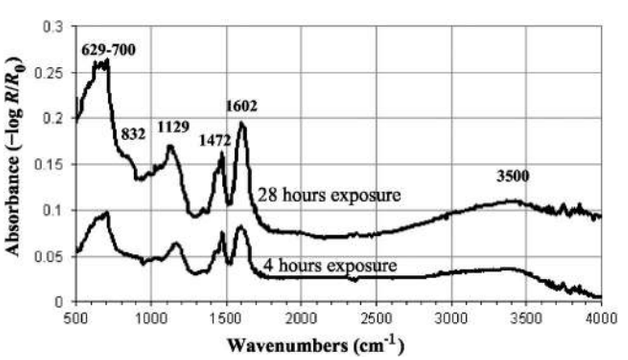

Figure 11. FTIR-IRAS spectra on EN W-3003 alloy obtained ex situ after 4 and 28 h exposure to a SWAAT solution at pH 4.0.

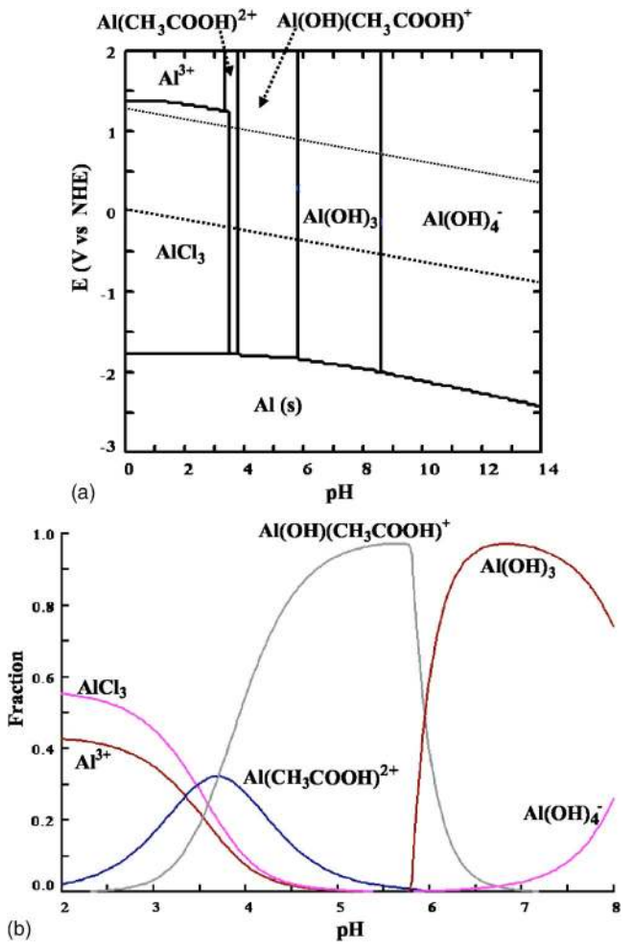

Figure 12. (Color online) (a) Pourbaix diagram for aluminum in an aqueous solution containing 1M NaCl and 0.1 M CH_3COOH. (b) Distribution (fraction) of aluminum species in this solution from pH 2 to 8 at the potential −0.6 V vs NHE.

between pH 3.8 – 5.8. With a further increase in pH, $Al(OH)_3$ and $Al(OH)_4^-$ become dominant, similar to aqueous systems without CH_3COOH.

The fraction of the dominant components depends strongly on the pH of the solution, as illustrated in Fig. 12b. $AlCl_3$ and Al^{3+} are the most predominant species in an acidic solution below pH 2. Their fractions decrease rapidly with increasing pH and diminish at around pH 5. The fraction of $Al(CH_3COOH)^{2+}$ increases with pH to reach a maximum value of about 0.3 at around pH 3.7, then decreases gradually and disappears at around pH 6. Meanwhile, the fraction of $Al(OH)(CH_3COOH)^+$ also begins to increase from pH 2.5 and becomes dominant above pH 4, until it drops drastically at a pH higher than ca. 5.7. The crystalline form of $Al(OH)_3$ is the dominant species at around pH 6–8 (near-neutral solutions).

The fraction of the dominant components in the aqueous solution at a given pH can be used for comparison with the IRAS results of the corrosion products deposited on the alloy surface. As an example, at pH 4, two aluminum acetate species are predominant in the solution at equilibrium conditions, with a fraction of about 0.28 for $Al(CH_3COOH)^{2+}$ and 0.52 for $Al(OH)(CH_3COOH)^+$, respectively. These species may adsorb and strongly bind to the hydrated alloy surface,[9,12,37] supporting the peak assignment of the IRAS spectra. $AlCl_3$ may exist in a small fraction (ca. 0.1), which is also in agreement with the IRAS results where $AlCl_3$ can hardly be detected. Moreover, in areas where local enhanced dissolution of Al^{3+} ions occurs (nonequilibrium condition), deposition of aluminum hydroxide and aluminum acetate compounds may occur locally, which was indeed observed by the in situ AFM measurements.

For the SWAAT solution at pH 2.9, the calculation indicates that the $AlCl_3$ is dominant (fraction ca. 0.46) and the fraction of $Al(CH_3COOH)^{2+}$ is also substantial (ca. 0.14), whereas the $Al(OH)(CH_3COOH)^+$ has only a minor fraction (ca. 0.02).

Corrosion mechanism and influence of IMPs.— Based on the combined information obtained from the OCP and EIS, integrated AFM/SECM, and in situ AFM measurements, as well as IRAS analysis and thermodynamic calculations, the electrochemical reactions involved in the corrosion process of the EN AW-3003 in the investigated solutions can be described as follows:

Anodic reaction

$$3Al \rightarrow Al^{3+} + 3e^- \quad [1]$$

This reaction, causing dissolution of aluminum, is enhanced in the boundary region adjacent to large IMPs (supported by in situ AFM observations) due to a galvanic action between the IMPs and the alloy matrix.[28]

Hydrolysis of Al^{3+} ions occurs in several steps in the bulk solution[8]:

$$Al^{3+} + H_2O \rightarrow Al(OH)^{2+} + H^+ \quad [2]$$

$$Al(OH)^{2+} + H_2O \rightarrow Al(OH)_2^+ + H^+ \quad [3]$$

$$Al(OH)_2^+ + H_2O \rightarrow Al(OH)_3 + H^+ \quad [4]$$

The cathodic reactions

$$O_2 + H_2O + 4e^- \rightarrow 4OH^- \quad \text{(near-neutral to neutral pH)} \quad [5]$$

$$2H^+ + 2e^- \rightarrow H_2(g) \quad \text{(acidic solutions)} \quad [6]$$

The reactions are enhanced on the exposed surfaces of the large IMPs due to their cathodic activity (AFM/SECM observations), leading to locally high concentrations of OH^-.[2,34] In acidic solutions, the total cathodic reaction rate is much higher due to the two reactions, Reactions 5 and 6, operating at the same time (OCP results). This may cause a locally high pH near the large IMPs, even in an acidic solution such as the SWAAT solution.

In the area around large IMPs, as a result of enhanced anodic dissolution and cathodic reaction on the IMPs, formation of corrosion products, e.g., $Al(OH)_3$, may occur locally (in situ AFM observations) in near-neutral solutions

$$Al^{3+} + 3OH^- \rightarrow Al(OH)_3 \quad [7]$$

Moreover, in the presence of acetic acid as in the SWAAT solution, the following reactions may occur, leading to formation of complexes like

$$Al^{3+} + CH_3COO^- \rightarrow Al(CH_3COO)^{2+} \quad [8]$$

$$Al^{3+} + CH_3COO^- + H_2O \rightarrow H^+ + Al(OH)(CH_3COO)^+ \quad [9]$$

This results in the formation of aluminum hydroxide and acetates that deposit locally on the alloy surface (in situ AFM observations, ex situ IRAS analysis), and the content of $Al(CH_3COOH)^{2+}$ and $Al(OH)(CH_3COOH)^+$ in the corrosion products depends on the pH (thermodynamic calculations).

The results from this work also elucidate the role of chloride ions in the corrosion mechanism of the aluminum alloy. In the near-neutral chloride solutions, although the OCP results and integrated AFM/SECM observations indicate that there are locally distributed events occurring on the alloy surface (Fig. 5-8), the EIS spectra suggest an overall passivelike behavior in these solutions. In contrast, in the acidic SWAAT solutions, the in situ AFM experiments show a much larger number of local active sites than in the near-neutral chloride solutions, in agreement with the EIS results that indicate a more active surface in the SWAAT solutions. Moreover,

for the SWAAT solution, the pH also has an influence on the corrosion reactions and formation of corrosion products. For the SWAAT solution at pH 4.0, thermodynamic calculation suggests that $AlCl_3$ is a minor component, and there is no clear peak in the IRAS spectra that could be assigned to chloride components. When the pH is 2.9, a substantial amount of $AlCl_3$ is expected to form on the surface. Although Cl^- alone can cause localized corrosion, these results suggest that extensive local dissolution only occurs when the Cl^- ions are in an acidic condition.

Regarding the influence of IMPs on the formation of the corrosion products, most studies in the literature concern pure aluminum or the alloys with Cu as a major alloying element, and aluminum chloride compounds were reported to form at locations related to Cu-rich IMPs,[2] especially in the presence of acetates.[29,30] In this work, the constituent IMPs in the EN AW-3003 alloy mainly contain Mn and Fe. In the SWAAT solution at pH 4.0 where extensive local dissolution occurs leading to formation of corrosion products, no direct evidence has been found for the involvement of Cl^- in the corrosion products formed on the alloy surface. It might be that Cl^- is only involved in the corrosion process as some intermediate species. However, when the pH is at 2.9, the corrosion products may contain a substantial fraction of $AlCl_3$. Furthermore, the thermodynamic calculations predict formation of $AlCl_3$ inside pits (where a high concentration of Cl^- and a low pH are expected), supporting the proposed pitting mechanism.[2] An in situ analytical technique with micrometer resolution is needed to detect anticipated aluminum chloride compounds formed inside pits.

Conclusions

To elucidate the influence of IMPs on localized corrosion of EN AW-3003 in near-neutral and acidic chloride solutions, this work combines conventional electrochemical measurements such as OCP and EIS, in situ microscopic observations of local electrochemical activity, and dissolution/precipitation by integrated AFM/SECM and in situ AFM imaging, ex situ IRAS analysis of corrosion products formed on the surface, and thermodynamic calculations of dominant regions of aluminum components in the system. The following conclusions can be drawn based on the results:

1. In situ microscopic probing of the alloy surface in the solutions by AFM and SECM provide detailed information about the action of IMPs in the localized corrosion of the aluminum alloy.
2. The in situ observations reveal that in near-neutral chloride solutions, localized dissolution occurs to a certain extent, preferably in the boundary region adjacent to some large IMPs, due to a galvanic effect by the oxygen reduction occurring on the IMPs. In acidic chloride solutions, the localized dissolution is greatly promoted by a strong galvanic action of the IMPs due to both the oxygen reduction and hydrogen evolution reactions, leading to many active sites and extensive localized dissolution on the alloy.
3. The enhanced local dissolution around IMPs and the cathodic reactions on the IMPs result in locally high concentrations of dissolved aluminum and hydroxyl ions, which facilitate formation and deposition of corrosion products around the IMPs, particularly in more acidic solutions. In the presence of acetate species, corrosion products consist of mixtures of aluminum oxihydroxide and acetate.
4. The formation and fraction of dominant species of the corrosion products depend on the pH of the solution, and aluminum chloride compounds may form at very low pH (below 4 for the solution investigated).

Acknowledgments

The authors thank Sapa Heat Transfer AB, Finspång, and the Brinell Center at the Royal Institute of Technology, Stockholm, for financial support. Dr. Ronggang Hu is acknowledged for contributions regarding the local electrochemical measurements.

The Royal Institute of Technology assisted in meeting the publication costs of this article.

References

1. G. S. Frankel, *J. Electrochem. Soc.*, **145**, 2186 (1998).
2. Z. Szklarska-Smialowska, *Corros. Sci.*, **41**, 1743 (1999).
3. N. Birbilis and R. G. Buchheit, *J. Electrochem. Soc.*, **152**, B140 (2005).
4. C. Gouveia-Caridade, M. I. S. Pereira, and C. M. A. Brett, *Electrochim. Acta*, **49**, 785 (2004).
5. T. Hurlen, H. Lian, O. S. Odegard, and T. Valand, *Electrochim. Acta*, **29**, 579 (1984).
6. H. J. W. Lenderink, M. V. D. Linden, and J. H. W. de Wit, *Electrochim. Acta*, **38**, 1989 (1993).
7. J. H. W. de Wit and H. J. W. Lenderink, *Electrochim. Acta*, **41**, 1111 (1996).
8. K. Sasaki and H. S. Isaacs, *J. Electrochem. Soc.*, **151**, B124 (2004).
9. T. E. Graedel, *J. Electrochem. Soc.*, **136**, 204C (1989).
10. J. Weissenrieder, C. Leygraf, M. Göthelid, and U. O. Karlsson, *Appl. Surf. Sci.*, **218**, 155 (2003).
11. B. F. Lewis, M. Mosesman, and W. H. Weinberg, *Surf. Sci.*, **41**, 142 (1974).
12. M. R. Alexander, G. Beamson, C. J. Blomfield, G. Leggett, and T. M. Duce, *J. Electron Spectrosc. Relat. Phenom.*, **121**, 19 (2001).
13. A. Ayral and J. C. Droguet, *J. Mater. Res.*, **4**, 967 (1989).
14. D. Persson and C. Leygraf, *J. Electrochem. Soc.*, **142**, 1459 (1995).
15. J. H. W. de Wit, *Electrochim. Acta*, **49**, 2841 (2004).
16. T. H. Muster and A. E. Hughes, *J. Electrochem. Soc.*, **153**, B474 (2006).
17. V. Guillaumin, P. Schmutz, and G. S. Frankel, *J. Electrochem. Soc.*, **148**, B163 (2001).
18. P. Schmutz and G. S. Frankel, *J. Electrochem. Soc.*, **146**, 4461 (1999).
19. G. O. Ilevbare, O. Schneider, R. G. Kelly, and J. R. Scully, *J. Electrochem. Soc.*, **151**, B453 (2004).
20. O. Schneider, G. O. Ilevbare, J. R. Scully, and R. G. Kelly, *J. Electrochem. Soc.*, **151**, B465 (2004).
21. C. H. Paik, H. S. White, and R. C. Alkire, *J. Electrochem. Soc.*, **147**, 4120 (2000).
22. J. C. Seegmiller and D. A. Buttry, *J. Electrochem. Soc.*, **150**, B413 (2003).
23. M. Buchler, J. Krimeo, F. Guillaume, and W. H. Smyrl, *J. Electrochem. Soc.*, **147**, 3691 (2000).
24. A. Davoodi, J. Pan, C. Leygraf, and S. Norgren, *Electrochem. Solid-State Lett.*, **8**, B21 (2005).
25. A. Davoodi, J. Pan, C. Leygraf, and S. Norgren, *Appl. Surf. Sci.*, **252**, 5499 (2006).
26. A. Davoodi, J. Pan, C. Leygraf, and S. Norgren, *Electrochim. Acta*, **52**, 7697 (2007).
27. J. C. Seegmiller, R. C. Bazito, and D. A. Buttry, *Electrochem. Solid-State Lett.*, **7**, B1 (2004).
28. A. Davoodi, J. Pan, C. Leygraf, and S. Norgren, *J. Electrochem. Soc.*, In press.
29. D. Chidambaram and G. P. Halada, *Surf. Interface Anal.*, **31**, 1056 (2001).
30. S. V. Kagwade, C. R. Clayton, D. Chidambaram, M. L. Du, and F. P. Chiang, *J. Electrochem. Soc.*, **147**, 4125 (2000).
31. A. Davoodi, J. Pan, C. Leygraf, Y. Zhu, and A. Farzadi, *J. Electrochem. Soc.*, Submitted.
32. I. Puigdomenech, Medusa—Chemical Equilibrium Software, Division of Inorganic Chemistry, Department of Chemistry, Royal Institute of Technology, Stockholm (2004).
33. R. Ambat, A. J. Davenport, G. M. Scamans, and A. Afseth, *Corros. Sci.*, **48**, 3455 (2006).
34. J. O. Park, C. H. Paik, Y. H. Huang, and R. C. Alkire, *J. Electrochem. Soc.*, **146**, 517 (1999).
35. K. Nisancioglu, *J. Electrochem. Soc.*, **137**, 69 (1990).
36. N. Le Bozec, D. Persson, A. Nazarov, and D. Thierry, *J. Electrochem. Soc.*, **149**, B403 (2002).
37. D. Tunega, G. Haberhauer, M. Gerzabek, and H. Lischka, *J. Phys. Chem. A*, **104**, 6824 (2000).